Journal of Food Measurement and Characterization
https://doi.org/10.1007/s11694-026-04081-8

ORIGINAL PAPER

Multi-objective genetic algorithm driven formulation of a plant-based probiotic premix powder: Nutrient-cost modeling, microstructural characterization and sensory validation

Ping Tang[1] · MingYang Cui[2] · Aliah Zannierah Mohsin[1] · Anis Shobirin Meor Hussin[1] · Nurul Hanisah Juhari[1]

Received: 2 December 2025 / Accepted: 13 January 2026

Abstract

This study presents a multi-objective genetic algorithm (NSGA-II) driven framework for the rational formulation of a plant-based probiotic premix powder under simultaneous nutritional and economic constraints. Protein content, energy value, and protein density were maximized while formulation cost was minimized within predefined macronutrient ranges. Pareto-optimal solutions were further refined into integer-feasible formulations and ranked using the Technique for Order Preference by Similarity to Ideal Solution (TOPSIS), from which the most balanced candidate was selected and experimentally validated. The predicted and measured nutritional values showed strong agreement, with relative errors below 6% for macronutrients, and approximately 6% for energy, confirming the robustness and practical reliability of the optimization strategy. During 28 days of storage, probiotic viability remained above 7 $\log_{10}$ CFU/g under refrigerated and ambient conditions, while elevated temperature accelerated viability loss and color changes.. Microstructural and physicochemical analyses revealed near-spherical particles and a predominantly amorphous composite matrix. Fourier transform infrared spectroscopy (FTIR) spectra confirmed the preservation of major carbohydrate–protein functional groups, while High-Resolution X-Ray Diffraction (XRD) patterns exhibited a broad diffraction halo without sharp crystalline peaks. Differential scanning calorimetry (DSC) thermograms displayed a single endothermic transition within the scanned temperature range, indicating good thermal stability of the composite matrix. Sensory evaluation further demonstrated acceptable flavor, viscosity, and overall preference of the optimized formulation. The novelty of this study lies in integrating multi-objective optimization, integer-feasible formulation refinement, and experimental validation into a single reproducible and cost-aware framework, offering a scalable strategy for the development of nutritionally optimized plant-based probiotic powders.

Keywords Multi-objective optimization · Plant-based porridge · Probiotic · Fermentation, Non-dairy alternative · Formulation · NSGA-II

✉ Anis Shobirin Meor Hussin
shobirin@upm.edu.my

Ping Tang
t1121p96@gmail.com

MingYang Cui
cuimingyang1997@163.com

Aliah Zannierah Mohsin
aliah_mohsin@upm.edu.my

Nurul Hanisah Juhari
n_hanisah@upm.edu.my

[1] Faculty of Food Science and Technology, Universiti Putra Malaysia, 43400 UPM Serdang, Selangor Darul Ehsan, Malaysia

[2] Department of Food Nutrition and Health, School of Food Engineering, East University of Heilongjiang, Harbin 150066, Heilongjiang, China

Published online: 25 February 2026

Introduction

Plant-based foods have gained increasing global attention as a strategic response to major challenges confronting contemporary food systems, including climate change, depletion of natural resources, and the growing demand for sustainable protein sources [1]. Mung bean, red kidney bean, and chickpea differ substantially in amino acid composition, starch structure, and micronutrient content, and their balanced combination has the potential to increase protein density, improve mouthfeel, and reduce bitterness [2]. Beyond their nutritional value, legumes contribute to sustainable agriculture through biological nitrogen fixation, improved soil fertility, and more efficient land and water use. As a result, legume-based foods are increasingly regarded as key components of future-oriented, sustainable dietary patterns.

In parallel with environmental and nutritional considerations, socio-economic factors such as food affordability, accessibility, and resource efficiency have become central to food system innovation [3]. Developing nutrient-dense yet cost-effective food products is particularly important for improving dietary quality and widening access to healthy food options across diverse consumer groups. In this context, blending different legumes offers a promising strategy to enhance nutritional complementarity. From a socio-economic perspective, formulation strategies that explicitly account for cost minimization are closely linked to public health, social welfare, and food and food accessibility [4]. Affordable, nutrient-dense food products are critical for improving dietary quality among low- and middle-income populations, where economic constraints often limit access to healthy foods. Technological innovation in food processing and formulation design therefore plays a pivotal role in fostering economic development and improving access to nutritious foods without compromising product quality. However, the behavior of multi-legume systems is highly composition-dependent. Variations in ingredient ratios can significantly affect energy contribution, textural properties, sensory perception, and overall cost structure, rendering empirical trial-and-error formulation inefficient and difficult to generalize. From a broader agri-food system perspective, these formulation challenges are closely linked to the efficient utilization of plant-based resources, cost control, and the development of affordable, nutrient-dense foods. In this regard, model-driven optimization approaches have been increasingly recognized as effective tools to support resource efficiency and evidence-based decision making in agricultural and food systems [5].

To address this challenge, multi-objective optimization provides a systematic strategy for food formulation. Nutritional products must achieve several goals at the same time, including high protein content, appropriate macronutrient ratios and reasonable cost. The non-dominated sorting genetic algorithm II (NSGA-II) can efficiently search within a constrained space and generate a Pareto set of optimal solutions [6]. Combined with the Technique for Order Preference by Similarity to Ideal Solution (TOPSIS), the most balanced formulation can be selected from all feasible candidates. Genetic algorithms have been widely adopted in materials and chemical engineering, yet their application in food product development is still emerging. Recent studies in related agri-food domains have further demonstrated that data-driven and optimization-based models can enhance decision making and policy design, underscoring the broader relevance of computational approaches for sustainable food system optimization [7]. Studies focusing on probiotic plant-based porridge powders derived from fermented legume milks are especially scarce.

This study aimed to develop an instant premix porridge powder by combining a spray-dried probiotic carrier derived from fermented legume milks with cooked powders of mung bean, red kidney bean and chickpea, together with selected food additives to improve sensory quality. NSGA-II and TOPSIS were employed to design a nutritionally balanced and cost-efficient formulation. The optimized powder was evaluated for proximate composition, probiotic viability, color and sensory attributes, while powder properties were characterized to assess microstructure, molecular interactions and thermal behavior. The findings provide technical evidence for a new generation of plant-based probiotic powders with improved convenience, nutritional density and shelf stability.

Materials and methods

Materials

Mung bean powder and chickpea powder were obtained from Henan Qingwen Food Co., Ltd (China). Red kidney bean powder was supplied by Jiangsu Junkanglai Health Industry Co., Ltd (China). Cocoa powder (Hershey's, USA) was purchased from AEON Supermarket (Malaysia), and konjac powder (RUIBIO, China) was used as the fiber source. De Man, Rogosa and Sharpe (MRS) broth and MRS agar (Brand, Country) were used for lactic acid bacteria cultivation and enumeration. All powders were stored in sealed containers at room temperature until use.

Preparation of plant-based probiotic powder

Plant-based probiotic powder was produced using fermented legume milk as the carrier, based on a preliminary study. Mung beans, kidney beans, and chickpeas were soaked overnight and homogenized with distilled water at a ratio of 1:8. The slurries were filtered through gauze, and the filtrates were refrigerated at 4 °C overnight to allow starch sedimentation, followed by decantation. Sucrose was added at 6%, and the samples were pasteurized at 90 °C for 15 min and cooled to room temperature. *Lactobacillus plantarum* PC4 was cultured in MRS broth at 37 °C, harvested by centrifugation at 3500 rpm for 3 min, and washed with sterile saline. Fermentation was conducted under conditions determined in preliminary experiments using a similar optimization workflow and selection criteria as previously reported [8]: mung bean milk was fermented for 6.0 h at 37.0 °C with 1.99% (v/v) inoculum; kidney bean milk was fermented for 6.46 h at 37.37 °C with 1.99% (v/v) inoculum; and chickpea milk was fermented for 7.40 h at 35.95 °C with 2.22% (v/v) inoculum. After fermentation, equal volumes of the three plant milks were combined, maltodextrin was added at 14.64% (w/v), gum Arabic was added at 1.04% (w/v), and the mixture was spray-dried using a Büchi B-290 dryer with an inlet temperature of 122 °C and a feed flow rate of 22%. Spray-drying conditions were determined in preliminary experiments using the same optimization and decision workflow applied in our fermentation study [8], and were guided by reported effects of inlet temperature and gum Arabic concentration on probiotic encapsulation [9].

MOGA for nutrition-cost trade-off optimization

Multi-objective genetic algorithm (NSGA-II) was employed to optimize the formulation of five plant-based ingredients including mung bean (x_1), kidney bean (x_2), chickpea (x_3), cocoa (x_4), and konjac powder (x_5). The decision vector was defined as Eq. (1), and the proximate composition of each ingredient used in the premix matrix is presented in Supplementary Table S1.

$$x = [x_1,\ x_2,\ x_3,\ x_4,\ x_5]^T \tag{1}$$

Each ingredient was bound based on processing feasibility, such that:

$$15 \le x_1 \le 30; 15 \le x_2 \le 30; 15 \le x_3 \le 30; 10 \le x_4 \le 20; 10 \le x_5 \le 20 \tag{2}$$

The total powder mass was fixed at 90 g, while probiotic powder remained constant at 10 g, therefore:

$$\sum_{i=1}^{5} x_i = 90 \tag{3}$$

Objective function formulation

For each candidate formulation, the nutritional values per 100 g product were calculated through linear blending. Total energy (E) was expressed as Eq. (4):

$$E = \frac{\sum_{i=1}^{5} E_i x_i + E_{pb}\, pb}{100} \tag{4}$$

Here, pb denotes probiotic powder.

The protein (P), fat (F), and carbohydrate (C) contents per 100 g of product were calculated by linear blending of ingredient contributions as shown in Eqs. (5)-(7), respectively:

$$P = \frac{\sum_{i=1}^{5} P_i x_i + P_{pb}\, pb}{100} \tag{5}$$

$$F = \frac{\sum_{i=1}^{5} F_i x_i + F_{pb}\, pb}{100} \tag{6}$$

$$C = \frac{\sum_{i=1}^{5} C_i x_i + C_{pb}\, pb}{100} \tag{7}$$

Protein density (PD) was calculated as Eqs. (8):

$$PD = 100\,\frac{P}{E} \tag{8}$$

The cost per 100 g product was computed as Eqs. (9):

$$Cost = \sum_{i=1}^{5} cost_i x_i \tag{9}$$

The optimization simultaneously maximized protein, energy, and protein density, while minimizing cost. To adapt these goals to NSGA-II, the objective vector was defined as Eqs. (10):

$$f(x) = (-P, -E, -PD, Cost) \tag{10}$$

Macronutrient feasibility constraints

To ensure nutritional relevance for healthy adults (aged 18–59 years), macro-ratio constraints were defined based on the Acceptable Macronutrient Distribution Ranges [10]. The protein contribution to total energy was restricted by:

$$0.15E \le 4P \le 0.30E \tag{11}$$

The limits for fat were:

$$0.07E \le 9F \le 0.16E \tag{12}$$

This range reflects the inherent low-lipid profile of legumes (typically < 6% fat) [2]. Higher dietary fat targets (20%–30% energy) were avoided to ensure mathematical feasibility for this oil-free, whole-legume system and to safeguard probiotic stability during spray drying. The constraints for carbohydrates were:

$$0.60E \leq 4C \leq 0.78E \tag{13}$$

This range reflects common regional dietary patterns in Asia [11]. Only candidates simultaneously satisfying Eqs. (11) to (13) were classified as nutritionally feasible.

NSGA-II configuration

NSGA-II was implemented using the gamultiobj solver in the MATLAB Global Optimization Toolbox. The algorithm was configured with a population size of 100 and a maximum of 300 generations. Scattered crossover was applied using the built-in crossoverscattered operator, in which each decision variable of the offspring is randomly inherited from one of the two parents. Mutation was performed using built-in mutationadaptfeasible operator, which adaptively adjusts mutation step sizes and directions while maintaining feasibility with respect to variable bounds and constraints. Crossover- and mutation-related options not explicitly specified were kept as MATLAB defaults.

The function tolerance was set to 10^{-6}, corresponding to the FunctionTolerance stopping criterion in MATLAB gamultiobj. According to MATLAB definition, this criterion does not directly impose an absolute tolerance on objective function values, but terminates the optimization when the change in the spread of the Pareto front across consecutive stall generations falls below the specified threshold. Because a fixed random seed was not enforced, convergence and robustness were evaluated through three independent runs using different random seeds.

Convergence was assessed using an Inverted Generational Distance (IGD) proxy computed against a common global reference Pareto set, where smaller IGD values indicate a closer approximation to the reference front. To ensure comparability across different population sizes and generation limits, a compact, discrete evaluation strategy was adopted rather than continuous convergence trajectories. Specifically, IGD values were recorded at generation 100, generation 250, and the final generation, together with runtime, the estimated plateau generation, and final-solution overlap. The corresponding convergence and robustness metrics are summarized in Table S2.

The solver generated a continuous Pareto set $\mathbf{X}_c$ and corresponding objective matrix F_c. Nutritional outcomes of each solution were recalculated and visualized in three-dimensional spaces of (P, E, PD) and (P, E, $Cost$).

MOEA/D configuration

Multi-objective evolutionary algorithm based on decomposition (MOEA/D) was applied as an alternative multi-objective solver. In MOEA/D, the multi-objective problem was decomposed into a set of scalar subproblems using a set of evenly spread weight vectors, and neighborhood relations among subproblems were defined by distances between weight vectors. Each subproblem was optimized by using information from its neighboring subproblems, and an external population was maintained to store nondominated solutions found during the search.

A population size of 100 was used, and each subproblem was assigned a neighborhood consisting of its 20 nearest weight vectors. Neighbor based mating was used with probability 0.9 to promote local search along adjacent weight directions, following the mating restriction mechanism described for MOEA/D, where the neighborhood size controls the balance between local exploitation and global exploration. Variation was implemented using differential evolution style operators with a scale factor of 0.5 and a crossover probability of 0.9 [12]. Because these operator hyperparameters are implementation dependent and are not fixed by the MOEA/D framework itself, a brief sensitivity check was conducted in the same manner as the NSGA-II convergence diagnostics, and a stable tradeoff between runtime and solution quality was selected for the final runs. The resulting MOEA/D Pareto set was then evaluated using the same integer neighborhood refinement, TOPSIS based ranking, and epsilon grid slimming procedures as described in Sections. "Integer neighborhood refinement" to "ε-grid slimming procedure", so that the post processing and selection criteria were kept identical across algorithms.

Integer neighborhood refinement

Since commercial formulations require integer gram units, each point in $\mathbf{X}_c$ was expanded into a discrete search neighborhood by integer perturbation. After rounding, all vectors were projected back into bounds and balanced to maintain Eq. (3). Solutions failing the constraints in Eqs. (11)-(13) were discarded, yielding an integer-feasible set $\mathbf{X}_i$.

TOPSIS-based ranking

To select the most balanced formulation, the Technique for Order Preference by Similarity to Ideal Solution (TOPSIS) was applied. The decision matrix was defined as Eq. (14):

$$X = [P,\ E,\ PD,\ Cost] \tag{14}$$

Vector normalization was applied as Eq. (15):

$$X_{norm} = \frac{X}{\|X\|} \tag{15}$$

Weights (w) were uniformly assigned as Eq. (16):

$$w = [0.25,\ 0.25,\ 0.25,\ 0.25] \tag{16}$$

The weighted normalized matrix was described as Eq. (17):

$$V = X_{norm} \circ w \tag{17}$$

The positive and negative ideal solutions were expressed as Eq. (18):

$$\begin{aligned} v_j^+ &= \begin{cases} \max(V_j), & \text{beneficial indicator} \\ \min(V_j), & \text{non-beneficial indicator} \end{cases} \\ v_j^- &= \begin{cases} \min(V_j), & \text{beneficial indicator} \\ \max(V_j), & \text{non-beneficial indicator} \end{cases} \end{aligned} \tag{18}$$

Distances to ideal solutions were computed by:

$$D^+ = \sqrt{\sum (V - v^+)^2}, D^- = \sqrt{\sum (V - v^-)^2} \tag{19}$$

The TOPSIS closeness coefficient (CC) was described as Eq. (20):

$$CC = \frac{D^-}{D^+ + D^-} \tag{20}$$

The formulation with the highest CC was selected as the best candidate.

ε-grid slimming procedure

To remove redundant solutions and retain representative Pareto points, ε-grid was applied to protein, energy, and protein density, as defined in Eqs. (21)–(23), with ε_P=0.10 g/100 g, ε_E=0.80 kcal/100 g, and ε_{PD}=0.010 g protein/100 kcal. This procedure was used solely as a post-processing step for redundancy reduction and did not affect dominance relationships or the TOPSIS-based optimality assessment.

$$bin_E = \left[\frac{P - P_{min}}{\varepsilon_P}\right] \tag{21}$$

$$bin_E = \left[\frac{E - E_{min}}{\varepsilon_E}\right] \tag{22}$$

$$bin_{PD} = \left[\frac{PD - P_{min}}{\varepsilon_{PD}}\right] \tag{23}$$

Within each grid cell, only the solution with the highest CC value was retained, resulting in a compact non-dominated integer Pareto frontier suitable for product development.

Proximate composition

Crude fat, ash, protein, moisture and carbohydrate were determined according to AOAC official methods (2000). The energy value of each formulation was calculated based on FAO guidelines (2003) using the Atwater conversion factors:

$$Energy\,(kcal/100g) = 4\,(Protein\%) + 9\,(Fat\%) + 4\,(Carbohydrate\%) \tag{24}$$

Shelf-life stability and probiotic viability of optimized premix porridge

Probiotic viability during storage

Shelf-life stability was evaluated under three storage temperatures to represent refrigerated storage, room-temperature storage, and accelerated thermal stress. Porridge powders were packed in food-grade polyethylene zipper-sealed pouches and tightly sealed prior to storage. Samples were stored at 4±1 °C, 27±2 °C, or 37±1 °C and analyzed on days 0, 7, 14, 21, and 28, defined as an initial one-month screening period for early post-production viability changes. For each sampling point, 1.0 g of powder was aseptically transferred into 9.0 mL of sterile physiological saline and vortexed for 2 min to obtain a homogeneous suspension. Serial tenfold dilutions were plated on MRS agar and incubated at 37 °C for 48 h. Plates containing 30–300 colonies were used for enumeration, and viable counts were expressed as $\log_{10}$ (CFU/g).

Determination of color

Color measurements were carried out using a Konica Minolta CR-300 reflectance colorimeter (Konica Minolta Sensing Inc., Japan) equipped with an 8 mm measuring aperture. The instrument was calibrated with a standard white plate before use, and measurements were performed on the legume-based milk samples at room temperature. Lightness (L*), redness (a*), and yellowness (b*) values were recorded according to the CIE Lab* color system.

Characterization of porridge premix powder

Cold Field emission scanning electron microscopy (SEM)

Microstructural analysis was conducted using a cold field emission SEM (SU8600, Hitachi, Japan). Powder samples were placed on conductive adhesive, gold-coated to enhance conductivity, and observed at 500×, 1000× and 5000× magnifications under an accelerating voltage of 1 kV.

Fourier transform infrared spectroscopy (FTIR)

The FT-IR spectra of optimized premix powder at neutral pH was measured at a range of 4000–400 cm^{-1} by a FT-IR Spectrometer (Bruker Invenio instrument) following the procedure described by [13].

High-resolution x-ray diffraction (XRD)

Crystalline characteristics were examined using an X-ray diffractometer (SmartLab 9 kW, Rigaku, Japan). Powdered samples were spread uniformly onto flat sample holders and lightly pressed to achieve a smooth surface. Diffraction profiles were recorded over a 2θ range of 5°−100° at a scan speed of 10°/min, with operating conditions of 40 kV and 40 mA.

Differential scanning calorimetry (DSC)

DSC analysis was carried out using a Discovery DSC 250 (TA Instruments, USA). Approximately 8–12 mg of premix powder was hermetically sealed in an aluminum pan, with an empty pan as the reference. The samples were heated from 30 °C to 300 °C at a constant heating rate of 10 °C/min under a nitrogen atmosphere. Thermal profiles were collected to evaluate glass transition and melting behavior.

Sensory evaluation

A semi-trained sensory panel (n = 14; 7 males and 7 females, aged 22–45 years) was recruited to evaluate the intensity of key sensory attributes of the reconstituted porridge samples using the generalized labeled magnitude scale (gLMS). Prior to formal evaluation, panelists participated in two structured training sessions (approximately 60 min each) designed to standardize attribute understanding and scale usage. Training included familiarization with the porridge matrix, clarification of sensory attribute definitions, and intensity alignment using food-based reference materials.

Four formulations were selected for sensory evaluation based on the multi-objective optimization outcome (Table 1). Each powder sample was reconstituted with warm water (40 ± 2 °C), stirred for 30 s, and served in odor-free cups coded with randomized three-digit numbers to ensure blind testing. All participants reported no history of food allergies, particularly to legumes, cereals, or dairy products, and provided informed consent prior to participation.

The gLMS ranged from 0 = "no sensation" to 9 = "strongest imaginable sensation of any kind," with intermediate verbal anchors (1 = barely detectable, 5 = moderate, 7 = strong). The gLMS was selected to enable sensitive discrimination of sensory intensity across formulations with substantially different nutritional density and structural characteristics, thereby minimizing ceiling effects and allowing quantitative comparison across attributes.

Panelists evaluated appearance uniformity, aroma intensity, acidity perception, thickness/viscosity, smoothness, flavor acceptability, and aftertaste intensity. During training, food-based reference standards were used for calibration: acidity was standardized using citric acid solutions (0.05% and 0.15%, w/v); thickness/viscosity was demonstrated using corn starch dispersions (0.5% and 2%, w/v); and smoothness was illustrated by comparing whole milk (smooth reference) with a diluted okara suspension (rough reference).

Sensory evaluations were conducted individually in a quiet, well-lit room free from extraneous odors. Bottled mineral water was provided for palate cleansing between samples, and discussion among panelists was not permitted during scoring. Sensory responses were recorded using paper ballots and subsequently digitized for statistical analysis. The study protocol was approved by the Ethics Committee of Universiti Putra Malaysia (Reference No.: JKEUPM-2025–284).

Statistical analysis

All experiments were performed in triplicate, and data are presented as mean ± standard deviation. Statistical significance was determined by one-way analysis of variance (ANOVA) followed by Tukey's multiple comparison test, with $p < 0.05$ considered significant. All statistical analyses, including optimization-related computations, were performed in MATLAB (MathWorks, USA).

Table 1 Selected formulations (F1-F4) for sensory evaluation with predicted nutritional values and cost

Sample	Mung bean/g	Kidney bean/g	Chickpea/g	Cocoa/g	Konjac/g	Probiotic powder/g	Energy (kcal/100 g)	Protein (g/100 g)	Fat (g/100 g)	Carb (g/100 g)	Protein Density (g/100 kcal)	Cost (MYR/100 g)
F1	19	19	30	12	10	10	367.31	20.56	2.90	69.33	5.60	2.79
F2	18	23	20	19	10	10	367.67	20.69	3.26	68.47	5.63	3.55
F3	20	18	30	12	10	10	367.32	20.55	2.89	69.35	5.60	2.78
F4	17	21	23	19	10	10	368.19	20.72	3.34	68.40	5.63	3.55

F1: formulation with the highest TOPSIS score, representing the overall optimal balance of protein, energy density, and cost

F2: formulation with the highest protein density (g protein per 100 kcal), representing the most protein-efficient sample

F3: formulation with the lowest production cost (MYR/100 g), representing the most economical option

F4: formulation with the highest caloric contribution (kcal/100 g), representing the energy-dense option

Results and discussion

Multi-objective optimization outcomes and selection of feasible formulations

The multi-objective NSGA-II algorithm produced a continuous Pareto front balancing protein, energy, protein density, and formulation cost under the predefined macronutrient constraints. All solutions satisfied the required nutritional window (protein 15–30% of energy, fat 7–16%, carbohydrate 60–78%) while keeping probiotic powder fixed at 10 g per 100 g product, indicating that nutrient balancing was achieved without violating regulatory targets.

Figure 1A presents the distribution of integer-feasible Pareto solutions in the three-dimensional space defined by protein, energy, and protein density. A strong positive association among the three nutritional variables is evident, with solutions forming a narrow and continuous cluster rather than scattered extremes. The color gradient represents the TOPSIS closeness coefficient, showing that higher-ranked solutions are located toward the upper region of the Pareto surface, where protein density increases in parallel with protein and energy. Importantly, the TOPSIS-selected solution (marked by a star) does not correspond to the extreme maximum of any single objective, confirming that the decision strategy favors a balanced compromise rather than unilateral optimization.

When formulation cost is introduced as an additional dimension (Fig. 1B), an explicit nutrition–cost trade-off becomes apparent. Although protein and energy remain positively correlated, solutions with comparable nutritional performance exhibit a pronounced spread in cost. The color mapping indicates that higher TOPSIS scores are more frequently associated with solutions located at the lower-cost side of the feasible region, highlighting cost as a discriminating factor within an otherwise narrow nutritional window. Accordingly, the selected optimal formulation is positioned in a region that maintains high nutritional performance while avoiding excessive cost.

The interrelationships among individual variables are further visualized in the pairwise scatter–histogram matrix shown in Fig. 1C. Protein, energy, and protein density display narrow unimodal distributions and strong linear correlations, reflecting stable nutritional behavior across integer-feasible solutions. In contrast, formulation cost exhibits a broader distribution and weaker correlations with the nutritional variables, indicating greater sensitivity to ingredient substitution rather than nutritional output. This difference explains why cost plays a critical role in differentiating otherwise similar formulations and supports the use of TOPSIS for selecting solutions that achieve both nutritional adequacy and economic practicality.

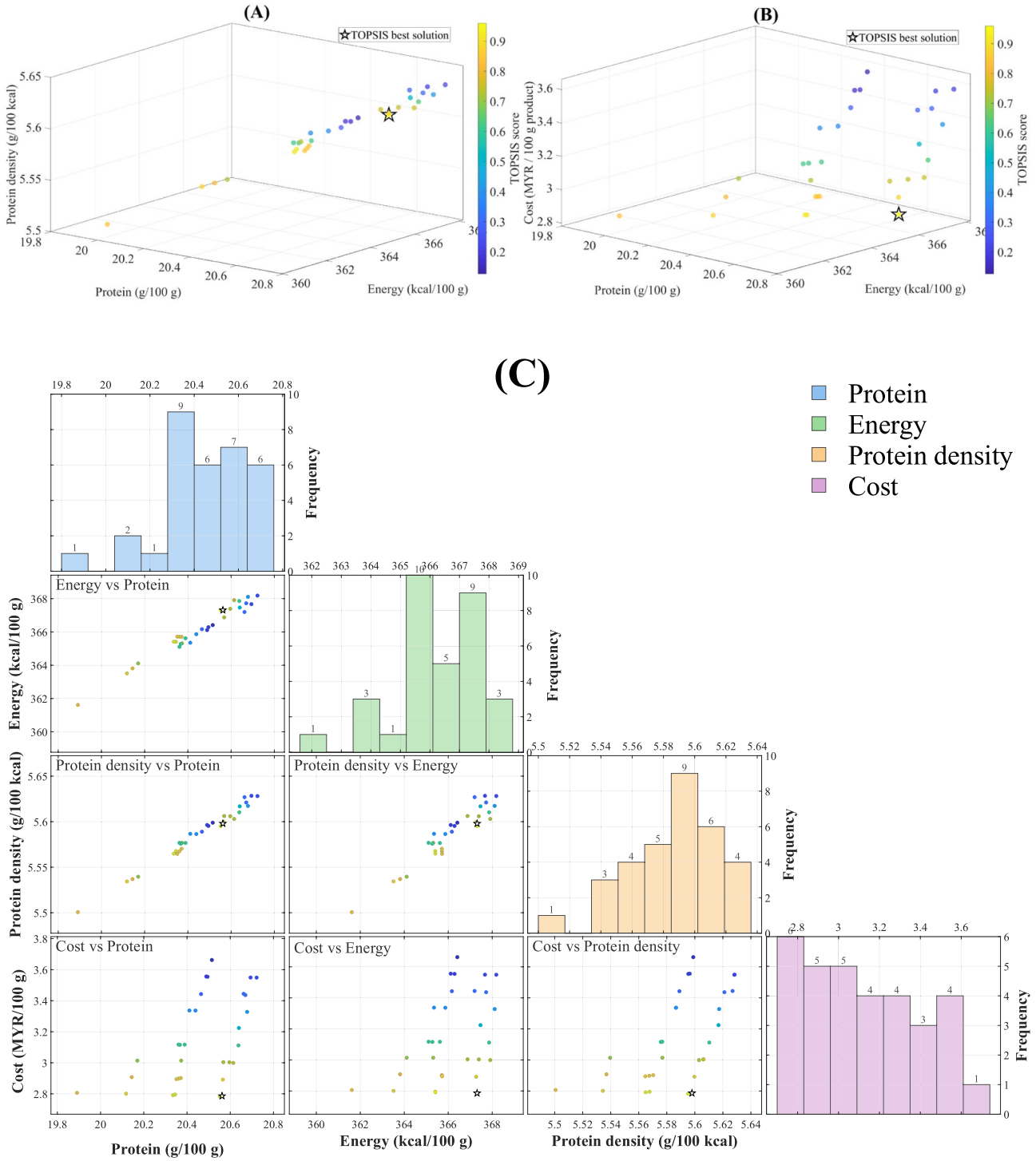

Fig. 1 Multi-objective trade-off visualization and TOPSIS selection of optimized formulations. (**A**) 3D distribution of feasible solutions in the protein, energy, and protein density space. Point color indicates the TOPSIS score, and the star marks the TOPSIS selected solution. (**B**) 3D distribution of feasible solutions in the protein, energy, and cost space. Point color indicates the TOPSIS score, and the star marks the TOPSIS selected solution. (**C**) Pairwise scatter–histogram matrix illustrating the distributions and bivariate relationships among protein (g/100 g), energy (kcal/100 g), protein density (g protein/100 kcal), and formulation cost (MYR/100 g) for all integer-feasible solutions. Diagonal panels show the frequency distributions of each variable. Off-diagonal panels present pairwise scatter plots, where each point represents one feasible formulation. Scatter points are colored according to the TOPSIS closeness coefficient

Table 2 Model-predicted nutritional composition and cost of representative integer-feasible formulations obtained from multi-objective optimization

(A) Representative solutions obtained from NSGA-II optimization (TOPSIS-based selection)											
Mung bean/g	Kidney bean/g	Chickpea/g	Cocoa/g	Konjac/g	Probiotic powder/g	Energy (kcal/100 g)	Protein (g/100 g)	Fat (g/100 g)	Carb (g/100 g)	Protein Density (g/100 kcal)	Cost (MYR/100 g)
19	19	30	12	10	10	367.31	20.56	2.90	69.33	5.60	2.79
20	18	30	12	10	10	367.32	20.55	2.89	69.35	5.60	2.78
18	19	30	12	11	10	365.41	20.35	2.89	69.55	5.57	2.80
19	18	30	12	11	10	365.42	20.34	2.88	69.57	5.56	2.79
18	18	30	12	12	10	363.51	20.12	2.87	69.80	5.53	2.80
20	19	28	13	10	10	367.27	20.57	2.93	69.24	5.60	2.89
20	16	30	13	11	10	365.72	20.35	2.97	69.44	5.56	2.89
19	17	30	13	11	10	365.71	20.36	2.97	69.42	5.57	2.89
18	18	30	13	11	10	365.71	20.37	2.97	69.41	5.57	2.90
18	17	30	12	13	10	361.61	19.89	2.86	70.04	5.50	2.81
(B) Representative solutions obtained from MOEA/D optimization											
Mung bean/g	Kidney bean/g	Chickpea/g	Cocoa/g	Konjac/g	Probiotic powder/g	Energy (kcal/100 g)	Protein (g/100 g)	Fat (g/100 g)	Carb (g/100 g)	Protein Density (g/100 kcal)	Cost (MYR/100 g)
15	16	30	19	10	10	369.39	20.78	3.51	68.23	5.63	3.55
15	15	30	20	10	10	369.69	20.81	3.61	68.08	5.63	3.65
16	15	30	19	10	10	369.39	20.77	3.52	68.25	5.62	3.54
15	22	23	20	10	10	368.47	20.77	3.43	68.21	5.64	3.66
17	15	30	18	10	10	369.10	20.74	3.43	68.41	5.62	3.43
17	15	29	19	10	10	369.22	20.76	3.49	68.28	5.62	3.54
15	20	27	18	10	10	368.57	20.74	3.36	68.43	5.63	3.44
15	22	24	19	10	10	368.35	20.75	3.37	68.34	5.63	3.56
16	17	30	17	10	10	368.79	20.72	3.34	68.54	5.62	3.33
17	16	30	17	10	10	368.80	20.17	3.34	68.56	5.62	3.33

The top ten ranked formulations are summarized in Table 2 (A). Energy ranged from 361.61 to 367.32 kcal/100 g, and protein ranged from 19.89 to 20.57 g/100 g, confirming the nutritional stability of the feasible region. Protein density remained consistently high (5.50–5.60 g/100 kcal), while fat content was naturally low (2.86–2.97 g/100 g), meeting the expectations of a low-fat, high-protein product. More variation was observed in cost (2.78–2.90 MYR/100 g), again highlighting that ingredient price, rather than nutritional value, was the primary driver of variability within the feasible space.

Comparing Table 2(A) and Table 2(B) reveals distinct ingredient profiles and cost outcomes. Formulations in Table 2(B) generally used more cocoa, which coincided with higher fat content and higher total cost, consistent with cocoa's composition and unit price rather than an optimization preference. In contrast, Table 2(A) shows lower and more concentrated cocoa inclusion, yielding reduced fat and lower cost. As both algorithms were run under identical objectives and constraints, these differences likely reflect algorithm-specific search and selection behavior rather than systematic bias. After integer rounding, NSGA-II produced a more discrete and sparse solution set, whereas MOEA/D retained a smoother, more continuous Pareto front (Fig. 2). This difference reflects their search strategies: MOEA/D explores along predefined weight directions, while NSGA-II depends on dominance and crowding, leaving fewer distinct non dominated combinations under integer constraints. Despite this, both methods converged to highly overlapping nutritional regions with similar ranges of protein, energy, and protein density. Thus, nutritional feasibility is robust, and residual differences in cocoa, fat, and cost mainly arise from

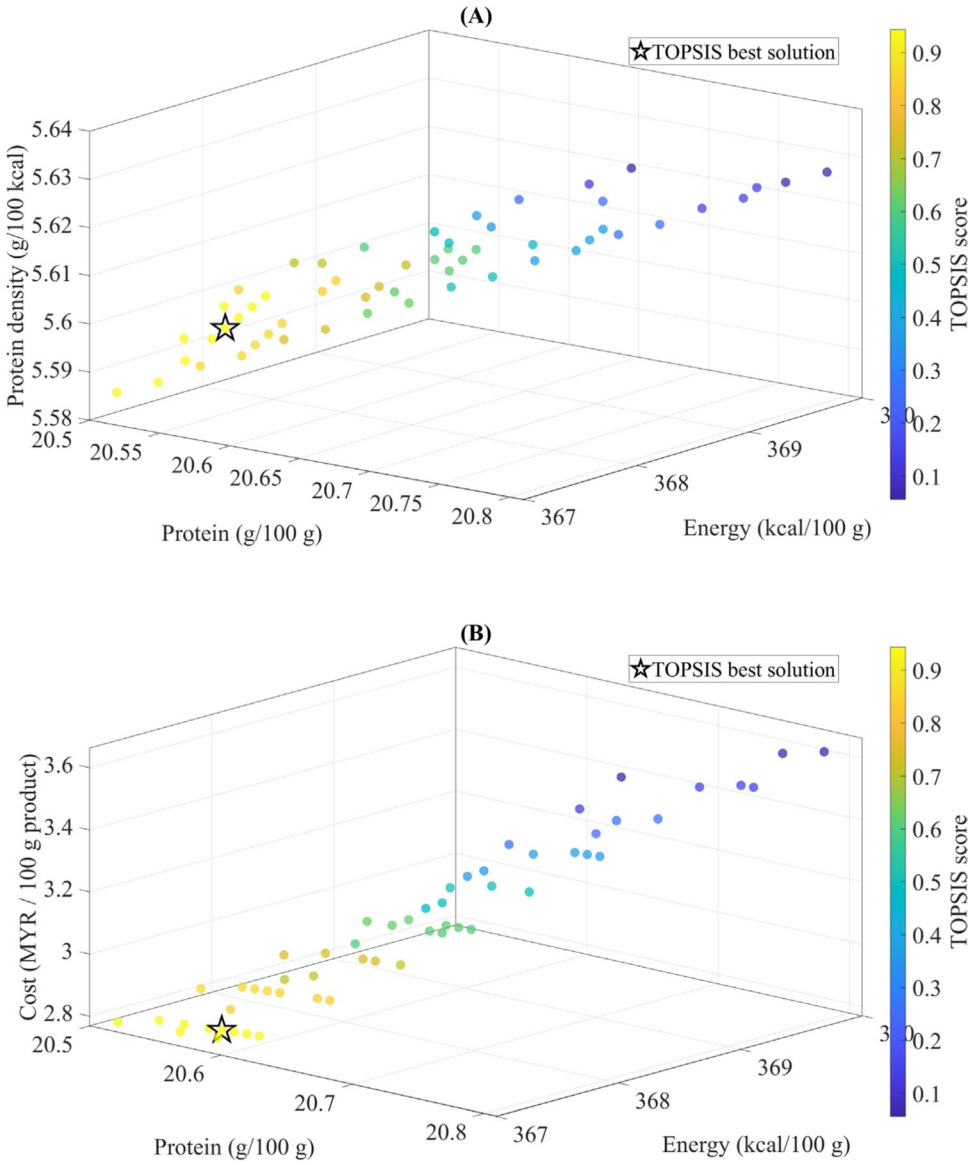

Fig. 2 3D Pareto representations of representative solutions obtained from MOEA/D optimization. (**A**) 3D distribution of MOEA/D-derived Pareto-optimal solutions in terms of protein content, energy value, and protein density. (**B**) 3D distribution of MOEA/D-derived Pareto-optimal solutions in terms of protein content, energy value, and cost. In both panels, solutions are color-coded according to their TOPSIS scores, and the star symbol indicates the TOPSIS-selected best compromise solution

algorithm dependent exploration under integer rounding rather than deliberate optimization toward sensory or economic attributes.

To provide a clear benchmark, three single-objective baselines were also solved under the same decision variables, total-mass constraint, and macronutrient feasibility window as those used in the NSGA-II framework. Protein-only maximization, cost-only minimization, and protein-density-only maximization were defined as the baseline cases. The resulting formulations and their predicted nutrition and cost metrics were reported in Supplementary Table S3. It was indicated that, within the restricted feasible region, only limited gains were achieved when a single target was optimized, whereas other key attributes were often weakened. By contrast, a compromise region was revealed by the multi-objective Pareto solutions, in which protein, energy, protein density, and cost were balanced simultaneously.

Validation of nutritional calculations against experimental measurements

Table 3 presents the experimental validation of the NSGA-II–selected optimal formulation by comparing deterministically calculated nutritional values with experimentally measured results. Overall, a high level of agreement was observed across all evaluated nutritional parameters, indicating that the formulation framework provides reliable nutritional estimates under the defined constraints.

Protein, fat, and carbohydrate contents exhibited very small deviations between calculated and measured values, with relative errors below 2.5%. These results indicate that the linear blending–based nutritional calculations accurately captured the macronutrient composition of the optimized formulation. To further strengthen the assessment beyond simple relative error, normalized error-based indicators were introduced. In particular, the relative root mean square error (RRMSE) and mean absolute percentage error (MAPE) were employed to facilitate comparison across nutritional parameters expressed in different units and magnitudes [14]. The use of RRMSE as a scale-independent metric has been widely recommended in the literature for cross-target performance comparison and error normalization. Similarly, MAPE has been frequently reported as a complementary indicator that provides intuitive, percentage-based interpretation of deviation across heterogeneous variables [15, 16].

Consistent with these methodological recommendations, the low RRMSE and MAPE values obtained for protein, fat, and carbohydrate further confirm the robustness of the calculation–experiment agreement for primary macronutrients. In contrast, energy and protein density exhibited moderately higher deviations, with relative errors of approximately 5–6%. This difference is primarily attributable to the sensitivity of energy-related indicators to ingredient-specific energy conversion assumptions rather than inaccuracies in formulation composition. In the present framework, the energy contribution of konjac powder was calculated using manufacturer-declared dietary fiber energy values, whereas experimental energy determination relied on the carbohydrate-by-difference method, in which dietary fiber and digestible carbohydrates cannot be analytically distinguished. As a result, even small discrepancies in dietary fiber energy conversion may propagate into total energy estimation, thereby amplifying deviations in both energy and derived protein density.

As summarized in Table S4, paired t-test analysis based on replicate experimental measurements ($n=3$) revealed no statistically significant differences between calculated and experimentally measured values for protein, fat, carbohydrate, and energy ($p>0.05$), indicating that the observed deviations for these parameters fall within the expected range of analytical variability. In contrast, protein density exhibited a statistically significant difference ($p<0.05$). The statistical significance observed for protein density is likely attributable to its dependence on energy as a normalization factor. Because protein density is a ratio-based parameter, minor systematic deviations in energy estimation may be amplified in the derived value, rather than reflecting inaccuracies in protein quantification itself.

Physicochemical changes of the optimal formulated premix porridge powder during storage

The physicochemical stability of the optimized premix porridge powder was assessed by probiotic viability and color parameters (L*, a*, b*) during 28 days of storage at 4 °C, 27 °C, and 37 °C (Figs. 3 and 4). Probiotic counts (Fig. 3) remained above 7 $\log_{10}$ CFU/g under all conditions. A slight increase on day 7, most evident at 37 °C, may be related to

Table 3 Experimental validation of the NSGA-II predicted optimal formulation

Parameter	Optimized predicted value	Experimental value	Error (%)	RRMSE (%)	MAPE(%)
Protein (g/100 g)	20.56	20.69±0.33	0.63	1.48	1.33
Fat (g/100 g)	2.90	2.97±0.12	2.36	4.16	3.89
Carbohydrate (g/100 g)	69.33	69.84±1.79	0.73	2.21	2.09
Energy (kcal/100 g)	367.31	388.87±9.63	5.54	5.90	5.51
Protein density (g/100 kcal)	5.60	5.32±0.10	5.26	5.49	5.29

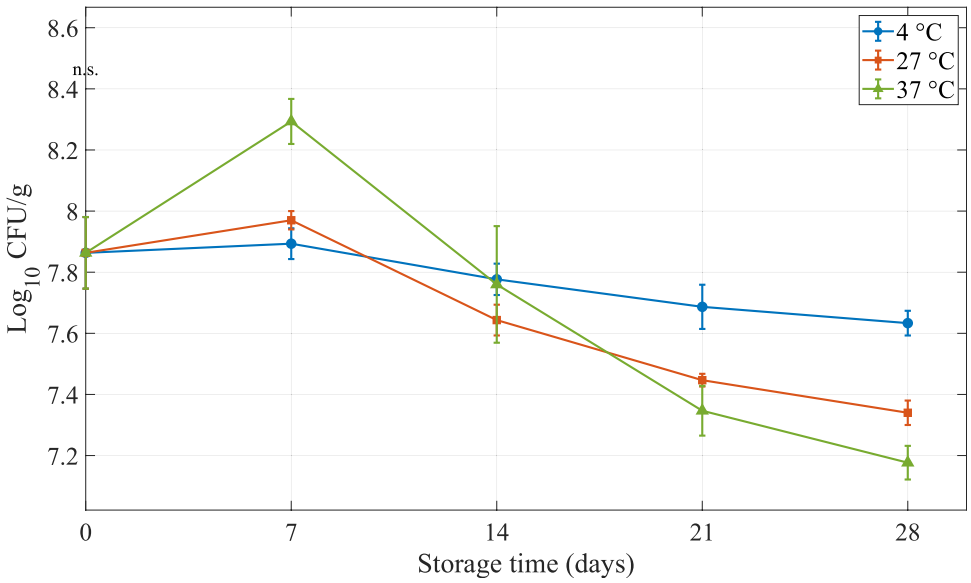

Fig. 3 Probiotics viability of optimal premix porridge powder during storage at 4 °C and 27 °C over 28 days. Data are presented as mean ± SD (n = 3). Asterisks indicate significant differences between the two storage conditions at the same time point (*p < 0.05, **p < 0.01, *p < 0.001)

the recovery of metabolically inactive cells. Thereafter, viability decreased in a temperature-dependent manner, with the smallest loss at 4 °C (about 0.25 $\log_{10}$ CFU/g), followed by 27 °C (about 0.6 $\log_{10}$ CFU/g) and 37 °C (about 0.7–0.8 $\log_{10}$ CFU/g) by day 28, indicating faster inactivation at elevated temperature.

Color changes showed consistent temperature effects (Fig. 4). L* and a* decreased over time, whereas b* increased, with the largest shifts at 37 °C and moderate changes at 27 °C, suggesting enhanced non-enzymatic browning and oxidative pigment changes at higher temperatures. Similar Maillard-related and oxidation-driven color evolution has been reported for protein–carbohydrate powder systems during storage [17].

Microstructure and particle morphology

SEM micrographs at 500×, 1000×, and 5000× magnification (Fig. 5) demonstrated a heterogeneous composite structure. Coarse, irregular legume particles coexisted with smaller, mostly spherical microcapsules derived from the spray-dried probiotic carrier. The powder showed a broad size distribution and a densely packed arrangement, indicating acceptable particle flow and limited inter-particle voids.

At 500×, coarse fragments were visible together with abundant fine particles. The dense packing and clustered groups suggested partial agglomeration formed during drying and handling. Occasional fractured edges were consistent with the presence of milled bean and cocoa solids.

At 1000×, satellite structures were clearly observed, where small spherical particles adhered to larger particles and formed neck-like connections. This morphology is commonly reported in spray-dried powders and can be attributed to droplet and particle adhesion during drying and subsequent particle–particle collisions. Given the spray-drying conditions used (inlet temperature 122 °C; feed flow rate 22%), the resulting surface roughness and agglomerated architecture may enhance wettability during reconstitution [18] and may also provide a physically protective, carbohydrate-rich matrix that helps limit direct exposure of embedded cells to oxygen and moisture.

At 5000×, microcapsule surfaces showed smooth glassy films alongside wrinkled or collapsed regions. These features likely resulted from fast moisture escape, internal vapor pressure, and limited shell strength of carbohydrate-rich matrices, such as maltodextrin and gum arabic. Smooth regions indicated successful film formation and potential embedding of probiotic cells, whereas localized collapse suggested brittleness after drying [19].

The three magnifications confirmed a multi-scale particle system. Coarse bean particles provide structural bulk and flowability, whereas fine microcapsules contribute to rapid dispersion in water. The satellite morphology reduces the proportion of loose fines, which may improve handling and reduce dusting. Evidence of microcapsule integrity suggests reduced exposure of probiotics to oxygen and humidity, supporting better stability during storage and rehydration [20].

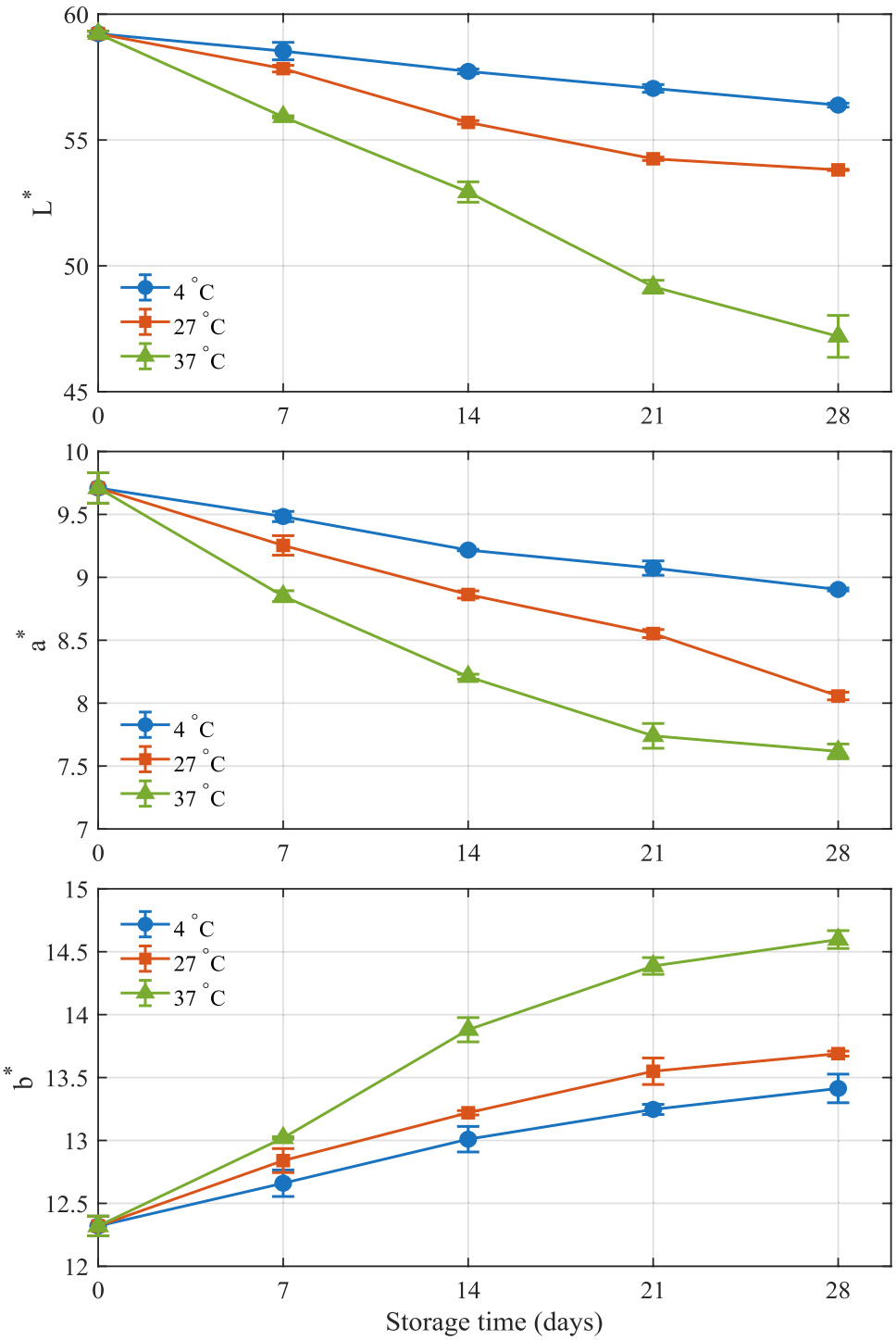

Fig. 4 Changes in L*, a*, and b* values of optimal premix porridge powder during storage at 4 °C and 27 °C over 28 days. Values represent mean ± SD (n = 3). Significant differences between storage temperatures at the same time point are indicated by asterisks (*p < 0.05, **p < 0.01, *p < 0.001)

FTIR structural characteristics

The FTIR spectrum (Fig. 6) of the optimized premix powder exhibited characteristic absorption bands associated with polysaccharide and organic backbone structures. The overall spectral profile appeared smooth and stable, indicating uniform composition and minimal baseline distortion. A weak absorption at 3001 cm^{-1} was attributed to aliphatic C–H stretching, reflecting the presence of hydrocarbon chains derived from plant proteins or residual lipids in the wall materials. The preservation of such hydrophobic structures suggests that spray drying did not cause severe degradation, which may benefit flavor retention and emulsifying stability [21].

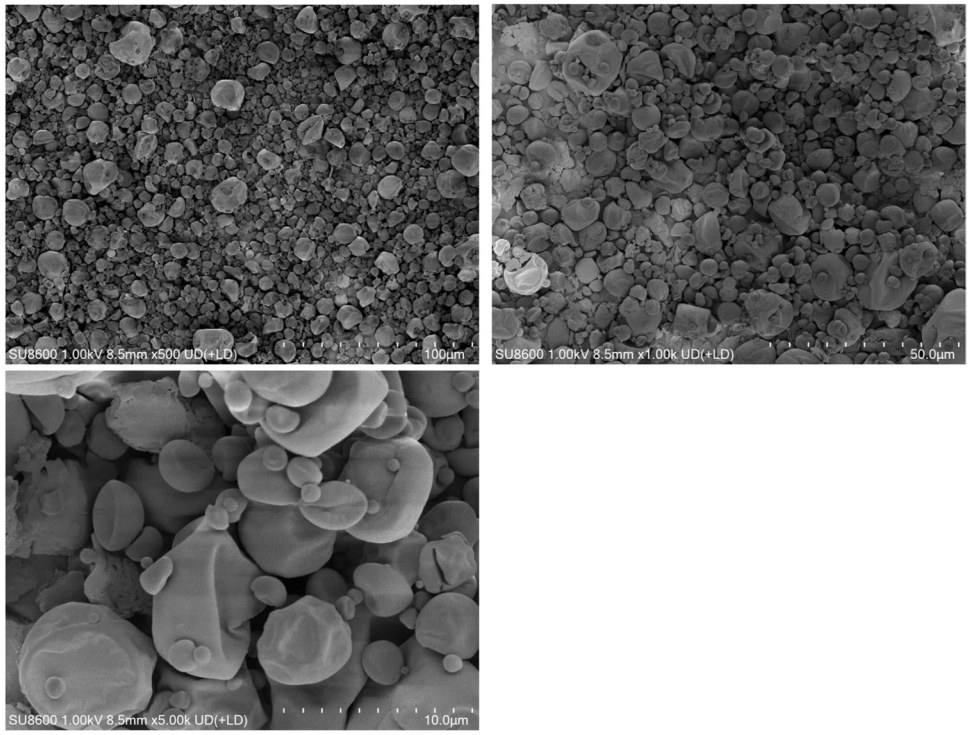

Fig. 5 SEM micrographs of the premix porridge powder at different magnifications (500×, 1000×, and 5000×)

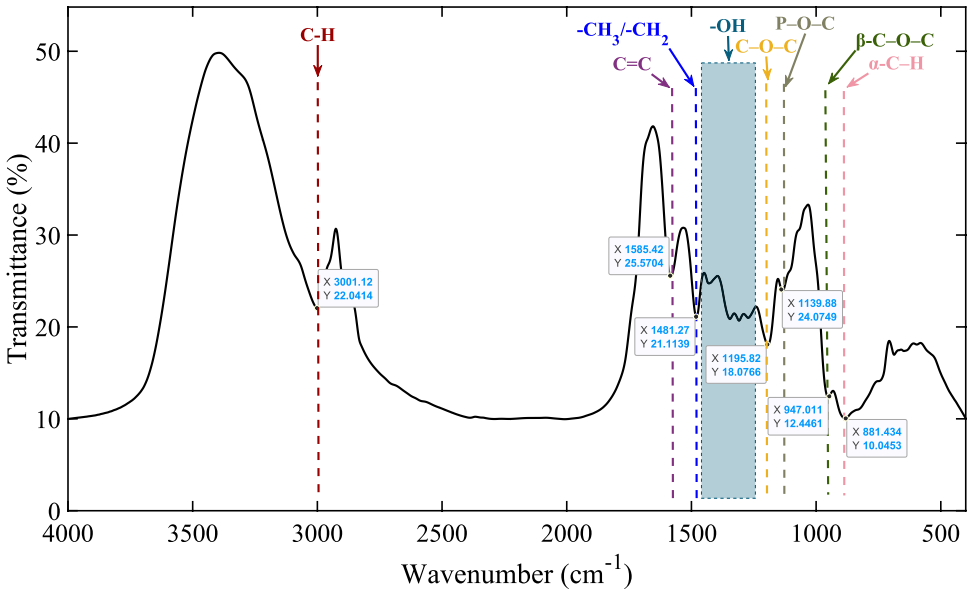

Fig. 6 FTIR spectrum of the optimal premix porridge powder

In the mid-infrared region, distinct peaks at 1585 cm^{-1} and 1481 cm^{-1} corresponded to C=C stretching and –CH_2/CH_3 bending vibrations, respectively [22].These signals confirm the persistence of stable organic carbon backbones, likely associated with protein and polysaccharide matrix segments. Their stability implies that thermal or dehydration-induced condensation reactions were limited, allowing structural integrity to remain high.

The most intense peak at 1195 cm^{-1} represented C–O–C stretching, a signature of polysaccharide linkages from maltodextrin and gum Arabic [23]. Its sharp and strong profile suggests a continuous glycosidic network that forms the main encapsulation framework, contributing to mechanical stability and moisture resistance. The band at 1139 cm^{-1}, assigned to P–O–C stretching, indicates the presence of phosphate-related groups, potentially from phospholipids or phosphate-bound amino residues [24]. Such interactions enhance the structural compactness and ionic balance of the powder matrix.

Lower-frequency peaks at 947 cm^{-1} and 881 cm^{-1} correspond to β-C–O–C glycosidic and α-C–H vibrations, respectively [25]. Their coexistence confirms that glycosidic

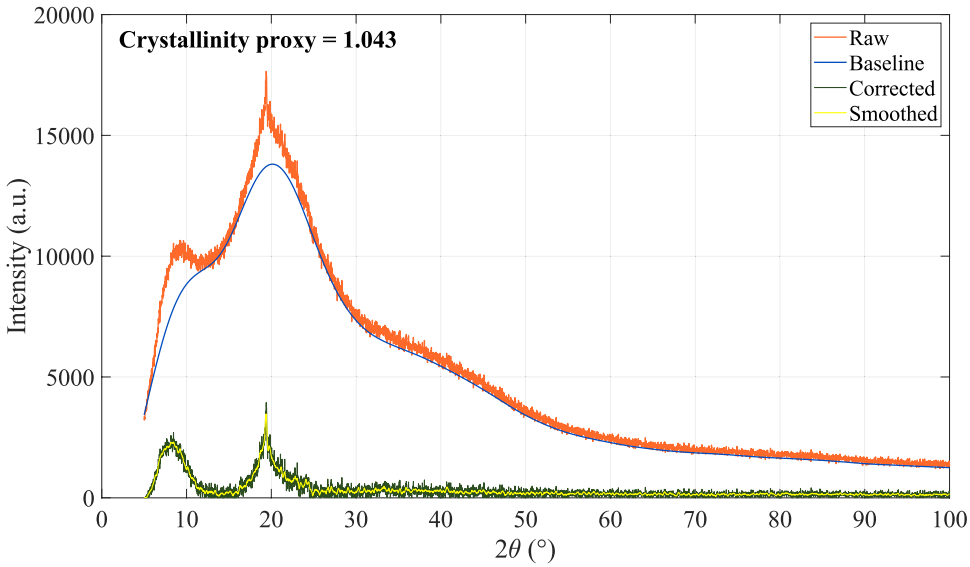

Fig. 7 XRD diffractogram of the optimized porridge premix powder

bonds remained intact, indicating minimal breakdown of polysaccharide chains during spray drying [26]. The preservation of β-glycosidic linkages is particularly important for maintaining the glassy matrix that protects probiotic cells and stabilizes the powder during storage [27].

X-ray diffraction analysis

Figure 7 shows the X-ray diffraction pattern of the optimized porridge premix powder. A broad amorphous halo spanning 10°–25° (2θ) dominated the diffractogram, reflecting the disordered structural nature of maltodextrin, konjac glucomannan, and cocoa polysaccharides [28]. Such a diffuse hump is typical for spray-dried carbohydrate matrices, where rapid moisture removal prevents molecular rearrangement and suppresses long-range crystallization [29]. The absence of sharp reflections indicates that the major structural components formed a continuous amorphous network rather than discrete crystalline domains. A small peak at approximately 19–20° (2θ) was still detectable, which is characteristic of the residual semi-crystalline lamellae in legume starch [30]. This suggests that a fraction of double-helix crystalline regions survived thermal gelatinization and shear exposure during slurry preparation [31]. In the present formulation, this minor crystalline contribution is expected to improve viscosity development and contribute to a smooth, cohesive texture during reconstitution [30]. Notably, no distinct reflections above 30° were observed, confirming the absence of mineral crystals or thermally stable crystalline impurities [32]. This is desirable for ready-to-mix powder products, as excessive crystallinity often reduces solubility and leads to sedimentation during dispersion. The predominantly amorphous state of the powder is consistent with its rapid hydration behavior, high wettability, and homogeneous dispersion when dissolved in hot water [33].

From a functional perspective, the amorphous matrix provides a high-energy, open structural arrangement that facilitates water penetration and swelling. Meanwhile, the limited starch crystallinity contributes to controlled thickening, preventing phase separation and maintaining colloidal stability during storage [34]. Together, these structural features indicate that the optimized formulation achieves a balance between instant solubility and texture formation, which is essential for consumer acceptability.

DSC analysis

Figure 8 shows the DSC thermogram of the optimized premix porridge powder. A distinct endothermic transition was observed, indicating structural changes of the biopolymer matrix during heating. The onset of thermal transition began at 31 °C, followed by a pronounced endothermic peak at 113 °C, and completed around 298 °C. The calculated enthalpy change (ΔH = 144) reflects the energy required for this thermal event.

This endothermic behavior is commonly associated with the loss of bound water and disruption of hydrogen bonding in starch–protein networks formed during processing [35]. The sharp decrease in heat flow near Tp suggests a relatively ordered structure that required higher thermal energy to dissociate [36]. Similar endothermic peaks have been reported in spray-dried and extrusion-processed cereal-based systems, particularly those with significant polysaccharide and legume-protein interactions [37]. The broad transition range (31–298 °C) implies a heterogeneous matrix containing components with different thermal stabilities, which is typical for multi-ingredient formulations.

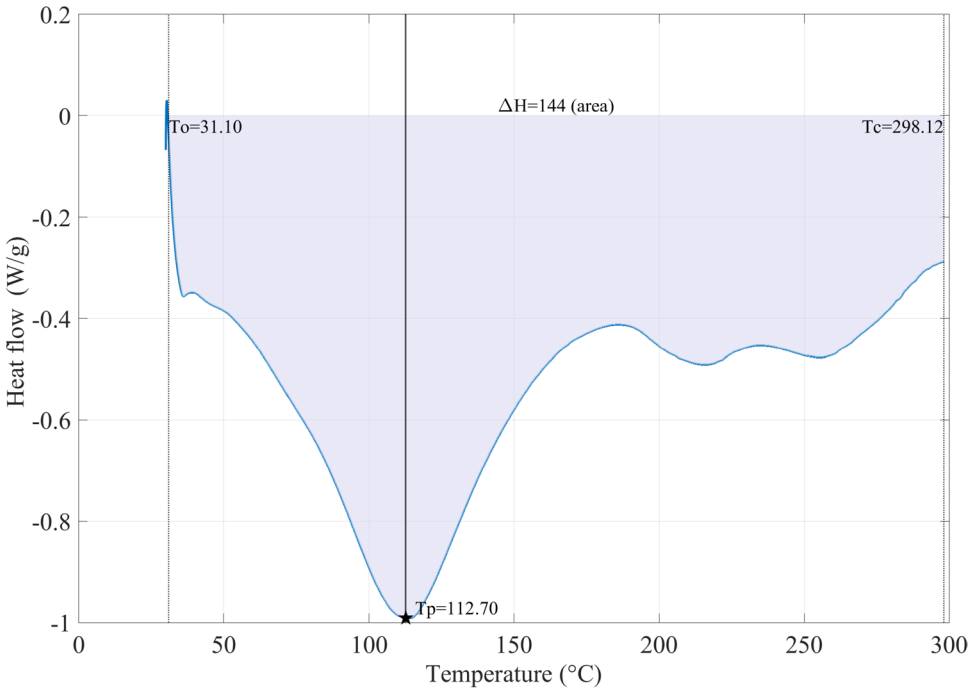

Fig. 8 DSC thermogram of optimized premix porridge powder, showing the onset temperature (To), peak temperature (Tp), and end temperature (Tc) of the main endothermic transition

The presence of a single dominant thermal event also indicates that no rapid degradation or crystallinity collapse occurred below 300 °C, suggesting good thermal stability for storage and reconstitution. The moderate ΔH value further supports that the powder maintains a stable amorphous or semi-amorphous state with sufficient molecular mobility for rehydration, while still resisting thermal degradation.

Sensory evaluation

Figure 9A presents the Principal Component Analysis (PCA) score plot and loading vectors of sensory attributes for the four formulations. PC1 and PC2 accounted for 36.4% and 19.6% of the total variance, respectively, demonstrating clear sensory differentiation among samples. F1, which achieved the highest TOPSIS score, was positioned near the central region of the PCA space, indicating a relatively balanced sensory profile across multiple attributes. This central positioning is consistent with its role as a compromise solution optimized simultaneously for protein density, energy contribution, and formulation cost, rather than being driven by the maximization of any single sensory attribute.

F2, characterized by the highest protein density, was clearly separated along the positive PC1 and negative PC2 axes and exhibited strong positive loadings for smoothness and thickness/viscosity. The elevated protein fraction likely enhanced mouth-coating and perceived body, explaining its dominance in texture-related attributes. F3, the most cost-efficient formulation, shifted toward the positive PC1 region and showed a close association with aroma intensity and aftertaste intensity, suggesting that cost minimization did not substantially impair flavor-related perception. F4, the most energy-dense formulation, clustered closer to the center with a mild association toward appearance uniformity, indicating stable reconstitution behavior and visual consistency.

Figure 9B summarizes the mean sensory scores using a radar plot. All formulations exhibited similarly high appearance uniformity and negligible acidity perception, indicating consistent reconstitution stability and the absence of sour off-notes across samples. F2 and F4 displayed higher aroma intensity and aftertaste intensity, which can be attributed to their higher cocoa powder content. However, this intensification of cocoa-derived notes was accompanied by lower flavor acceptability scores, likely due to increased bitterness, highlighting a sensory trade-off between aroma intensity and overall palatability.

Notably, although F1 achieved the highest flavor acceptability score, it exhibited the lowest smoothness score among the four formulations. This reduced smoothness can be attributed to formulation composition and particle-level structural characteristics rather than being a speculative effect. Chickpea-derived powders are known to contain relatively high levels of insoluble dietary fiber and rigid cell wall components, which are often retained during milling and dry fractionation processes. As summarized by Yeasmen and Orsat [38], chickpea flours and protein ingredients typically exhibit coarser particle size distributions and strong cell wall integrity, leading to incomplete hydration of cell wall polysaccharides and residual cotyledon fragments upon reconstitution. These structural features have been reported to increase particulate perception and surface roughness in

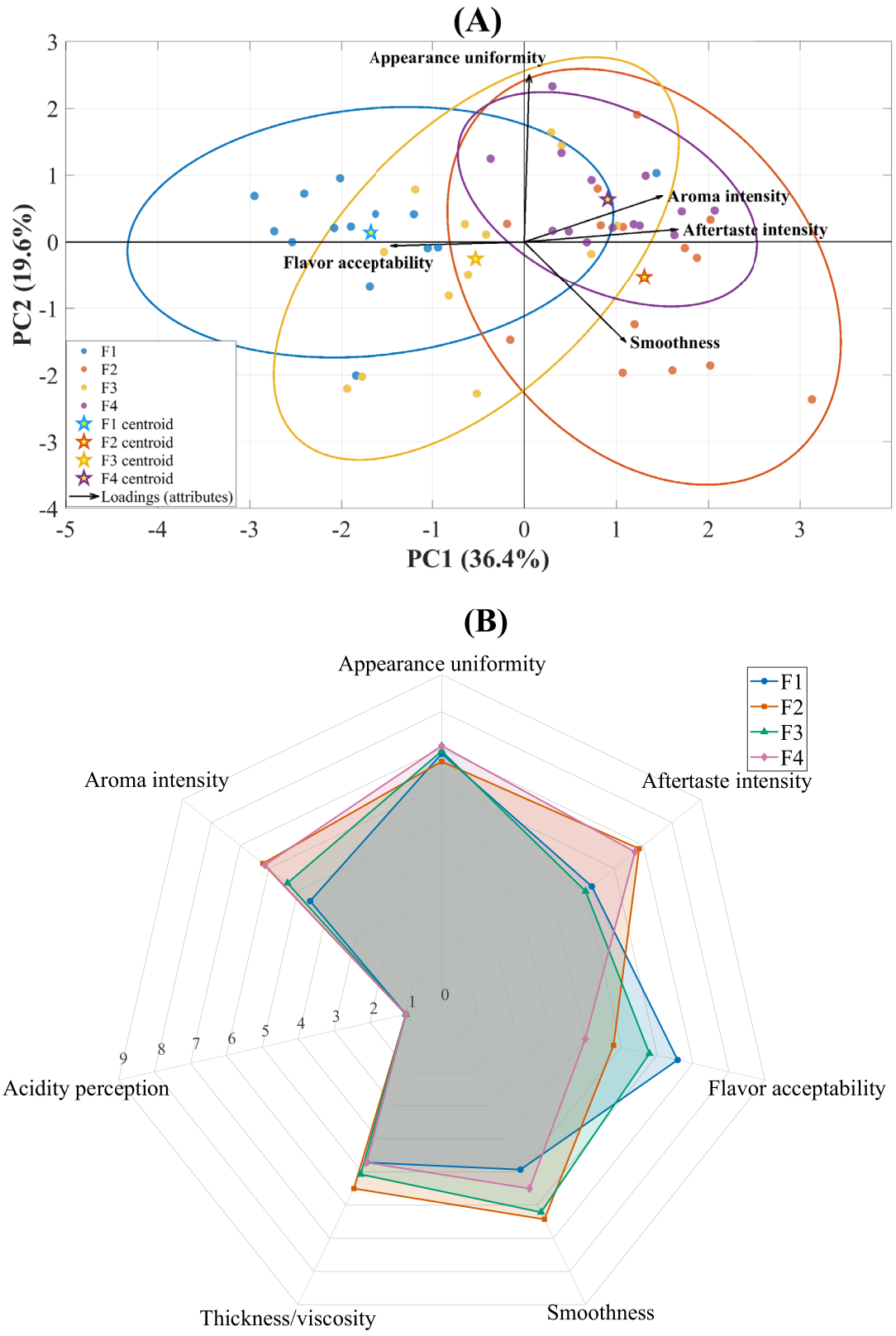

Fig. 9 PCA biplot (**A**) and radar chart (**B**) of sensory evaluation for samples F1–F4

liquid and semi-solid food matrices, such as soups, beverages, and porridge-type systems, particularly when thermal or mechanical size reduction is limited. Consistent with this interpretation, the SEM images (Fig. 4) at different magnifications show that the chickpea-rich formulation (F1) presented irregular flake-like and aggregated particle morphologies, with smaller particles frequently adhering to the surfaces of larger ones; such hierarchical and heterogeneous structures are typical of legume powders and are commonly associated with intact cell wall fragments and complex protein–polysaccharide matrices.

Implications for sustainable food system design

The findings of this study extend beyond single-formulation optimization and highlight the value of model-driven strategies in sustainable food system design. By integrating nutritional performance, cost constraints, and experimental validation within a unified multi-objective framework, the proposed approach enables rational decision-making under realistic formulation conditions. Compared with traditional response surface methodology, which often requires extensive experimentation for multi-component and constraint-rich systems, the MOGA-based strategy allows large-scale in silico screening using model-predicted responses. The resulting Pareto front explicitly reveals the trade-offs between nutritional quality and formulation cost, underscoring that improvements in nutritional density do not necessarily coincide with increased economic input. Such trade-off structures are increasingly recognized as intrinsic to sustainable food systems, where health, affordability, and production efficiency must be balanced simultaneously [39, 40].

The close agreement between predicted and experimental values further confirms the practical reliability of the modeling framework. By shifting formulation-space exploration from laboratory trial-and-error to computational screening followed by targeted validation, the proposed strategy substantially reduces experimental time, material consumption, and overall development cost. This reduction in resource use while maintaining nutritional adequacy and product quality directly supports the broader objectives of sustainable food production, including improved access to affordable, nutrient-dense foods and more responsible use of raw materials.

In this context, the present work is aligned with key global sustainability priorities, particularly those related to food security, public health, and responsible production. The development of a cost-efficient, nutritionally balanced, plant-based probiotic premix contributes to improving dietary quality and accessibility, while the use of optimization-driven formulation design enhances resource efficiency and minimizes unnecessary experimental waste. Notably, the robustness of the decision-making process under different stakeholder priorities was further supported by the weight sensitivity analysis (Table S5), which showed high consistency in formulation ranking across nutrition- and cost-oriented scenarios. Together, these outcomes demonstrate how computational decision frameworks can support the transition toward more sustainable and resilient food systems.

Conclusions

This study established a cost-aware, multi-objective optimization framework for the rational formulation of a plant-based probiotic premix powder under realistic nutritional constraints. By integrating NSGA-II optimization, integer-feasible refinement, and TOPSIS ranking, a balanced formulation was identified and experimentally validated, showing strong agreement between predicted and measured nutritional values. The optimized powder maintained probiotic viability above 7 $\log_{10}$ CFU/g during 28 days of storage, exhibited a predominantly amorphous structure with acceptable thermal stability, and achieved favorable sensory acceptance. Overall, the proposed framework provides a transparent and transferable strategy for developing nutritionally optimized, economically feasible plant-based probiotic powders.

Supplementary Information The online version contains supplementary material available at https://doi.org/10.1007/s11694-026-04081-8.

Acknowledgements The authors gratefully acknowledge the support and generosity of Universiti Putra Malaysia

Authors' contributions Ping Tang: Methodology, Investigation, Data curation, Writing-original draft, Formal analysis.
MingYang Cui: Methodology.
Aliah Zannierah Mohsin, Nurul Hanisah Juhari: Supervision.
Anis Shobirin Meor Hussin: Conceptualization, Supervision.

Funding Open access funding provided by The Ministry of Higher Education Malaysia and Universiti Putra Malaysia. This work was supported by Universiti Putra Malaysia through the Geran Universiti Putra Malaysia (GP/2024/9792200). The study was carried out under the Universiti Research Development Program (URDP) — Functional Food Development & Future Food research group.

Data availability The data that support the findings of this study are available from the corresponding author upon reasonable request.

Declarations

Competing interest The authors declare that they have no competing financial interests or personal relationships that could have influenced the work presented in this paper.

References

1. B. Sionek, A. Szydłowska, Probiotics and prebiotics in the aspect of health benefits and the development of novel plant-based functional food. Applied Sciences **15**(6), 3137 (2025)
2. Z. Ahmed, Optimization the nutrient composition and anti-nutrient of cereal-legume mixtures for infant complementary feeding: a review. Am. J. Food Sci. Technol. **4**(1), 60–66 (2025)
3. B. Jin, X. Xu, Machine learning wholesale white wheat price index forecasts. Qual. Quant. **30**, 1–29 (2025)
4. B. Jin, X. Xu, Predictive modeling of peanut oil prices utilizing a Gaussian process regression-based machine learning framework. Adv. Data Sci. Adapt. Anal. (2025). https://doi.org/10.1142/S2424922X25500068
5. X. Xu, Y. Zhang, Canola and soybean oil price forecasts via neural networks. Adv. Comput. Intell. **2**(5), 32 (2022)
6. Z. Zhou, Z. Lin, Y. Ma, J. Niu, J. Liu, X. Wang, Optimal design of colour formulation prediction for cotton fabrics based on NSGA-II and TOPSIS. Color. Technol. **141**(1), 63–79 (2025)
7. B. Jin, X. Xu, Late and early indica rice's price forecasts through neural networks. International Journal of Big Data Mining for Global Warming **07**(02), 2550005 (2025)
8. Ping T, Mohsin AZ, Juhari NH, Hussin ASM. 2025 Comparative machine learning strategies for improving antioxidant properties and aroma quality in fermented mung bean milkby Lactobacillus plantarum PC4. Int J Food Microbiol 111443.
9. D. Arepally, T.K. Goswami, Effect of inlet air temperature and gum Arabic concentration on encapsulation of probiotics by spray drying. LWT **99**, 583–593 (2019)
10. Dietary Reference Intakes for Energy, *Carbohydrate, fiber, fat, fatty acids, cholesterol, protein, and amino acids* (National Academies Press, Washington, D.C., 2005)
11. S. Henson, Linear programming analysis of constraints upon human diets. J. Agric. Econ. **42**(3), 380–93 (1991)
12. Q. Zhang, H. Li, MOEA/D: a multiobjective evolutionary algorithm based on decomposition. IEEE Trans. Evol. Comput. **11**(6), 712–731 (2007)
13. M. Cui, T.B. Tan, M. Fu, Z. Cheng, M. Mat Yusoff, C.P. Tan, Preparation and characterisation of palm-based tocotrienol-carotenoid emulsion stabilised by hemp protein isolate-ginsenoside emulsifier. Int. Food Res. J. **32**(3), 889–902 (2025)
14. B. Jin, X. Xu, Machine learning price index forecasts of flat steel products. Miner. Econ. **38**(1), 97–117 (2025)
15. X. Xu, Y. Zhang, China mainland new energy index price forecasting with the neural network. Energy Nexus **1**, 10 (2023)
16. B. Jin, X. Xu, China commodity price index (CCPI) forecasting via the neural network. Int. J. Financ. Eng. (2025). https://doi.org/10.1142/S2424786325500033
17. E.A. Norwood, C. le Floch-Fouéré, V. Briard-Bion, P. Schuck, T. Croguennec, R. Jeantet, Structural markers of the evolution of whey protein isolate powder during aging and effects on foaming properties. J. Dairy Sci. **99**(7), 5265–5272 (2016)
18. M. Yin, M. Chen, Y. Yuan, F. Liu, F. Zhong, Encapsulation of *Lactobacillus rhamnosus* GG in whey protein isolate-shortening oil and gum Arabic by complex coacervation: enhanced the viability of probiotics during spray drying and storage. Food Hydrocolloids **146**, 109252 (2024)
19. D. Arepally, R.S. Reddy, T.K. Goswami, Encapsulation of *Lactobacillus acidophilus* NCDC 016 cells by spray drying: characterization, survival after in vitro digestion, and storage stability. Food Funct. **11**(10), 8694–8706 (2020)
20. D.Y. Ying, M.C. Phoon, L. Sanguansri, R. Weerakkody, I. Burgar, M.A. Augustin, Microencapsulated *Lactobacillus rhamnosus* GG powders: relationship of powder physical properties to probiotic survival during storage. J. Food Sci. **75**(9), E588-95 (2010)
21. S. Dutta, C. Hartkopf-Fröder, K. Witte, R. Brocke, U. Mann, Molecular characterization of fossil palynomorphs by transmission micro-FTIR spectroscopy: implications for hydrocarbon source evaluation. Int. J. Coal Geol. **115**, 13–23 (2013)
22. M. Starsinic, R.L. Taylor, P.L. Walker, P.C. Painter, FTIR studies of Saran chars. Carbon **21**(1), 69–74 (1983)
23. M.S.M. Meiguni, M. Salami, K. Rezaei, M.A. Aliyari, S.B. Ghaffari, Z. Emam-Djomeh et al., Fabrication and characterization of a succinyl mung bean protein and arabic gum complex coacervate for curcumin encapsulation. Int. J. Biol. Macromol. **224**, 170–180 (2023)
24. R. Kwiatkowski, A. Włochowicz, Conformation and packing of poly(alkylene phosphate) chains in the crystal lattice. Part II: temperature FTIR studies. J. Mol. Struct. **516**(1), 57–69 (2000)
25. J. Chen, M. Zhou, L. Chen, C. Yang, Y. Deng, J. Li et al., Evaluation of physicochemical properties and prebiotics function of a bioactive *Pleurotus eryngii* aqueous extract powder obtained by spray drying. Nutrients **16**(11), 1555 (2024)
26. A. Ohja, S. B.G., H.A. Pushpadass, M.E.E. Franklin, C.R. Grover, S. Kumar et al., Encapsulation of *Lactiplantibacillus plantarum* CRD7 in sub-micron pullulan fibres by spray drying: maximizing viability with prebiotic and thermal protectants. Int. J. Biol. Macromol. **269**, 132068 (2024)
27. S. Misra, P. Pandey, C. Panigrahi, H.N. Mishra, A comparative approach on the spray and freeze drying of probiotic and Gamma-aminobutyric acid as a single entity: characterization and evaluation of stability in simulated gastrointestinal conditions. Food Chem. Adv. **3**, 100385 (2023)
28. L. Zhang, X. Zeng, N. Fu, X. Tang, Y. Sun, L. Lin, Maltodextrin: a consummate carrier for spray-drying of xylooligosaccharides. Food Res. Int. **106**, 383–393 (2018)
29. M.I. Amaro, L. Tajber, O.I. Corrigan, A.M. Healy, Co-spray dried carbohydrate microparticles: crystallisation delay/inhibition and improved aerosolization characteristics through the incorporation of hydroxypropyl-β-cyclodextrin with amorphous raffinose or trehalose. Pharm. Res. **32**(1), 180–195 (2015)
30. N. Singh, Y. Nakaura, N. Inouchi, K. Nishinari, Structure and viscoelastic properties of starches separated from different legumes. Starch - Stärke. **60**(7), 349–357 (2008)
31. X. Zhang, C. Zhu, D. Geng, Y. Cheng, N. Tang, Characterization of dynamic of the structural changes of legume starches during gelatinization. Int. J. Biol. Macromol. **296**, 139673 (2025)
32. M. Neuwirth, S.K. Kappes, M.U. Hartig, K.G. Wagner, Amorphous solid dispersions layered onto pellets—an alternative to spray drying? Pharmaceutics. **15**(3), 764 (2023)
33. J. Varshosaz, M. Minayian, M. Ahmadi, E. Ghassami, Enhancement of solubility and antidiabetic effects of Repaglinide using spray drying technique in STZ-induced diabetic rats. Pharm. Dev. Technol. **22**(6), 754–763 (2017)

34. X. Shi, Q. Zhong, Crystallinity and quality of spray-dried lactose powder improved by soluble soybean polysaccharide. LWT **62**(1), 89–96 (2015)
35. T. Piyapattanamongkol, V. Kongpensook, K. Tananuwong, Physicochemical properties and viscoelastic behavior of rice–mung bean composite flour systems as potential ingredients for plant-based foods. Cereal Chem. **99**(6), 1261–1271 (2022)
36. Md.M.R. Khan, P. Yu, Thermal stability and molecular microstructure of heat-induced cereal grains, revealed with raman molecular microspectroscopy and differential scanning calorimetry. J. Agric. Food Chem. **61**(26), 6495–504 (2013)
37. Md..K.. Haque, Y.H. Roos, Differences in the physical state and thermal behavior of spray-dried and freeze-dried lactose and lactose/protein mixtures. Innov. Food Sci. Emerg. Technol. **7**(1–2), 62–73 (2006)
38. N. Yeasmen, V. Orsat, Industrial processing of chickpeas (*Cicer arietinum*) for protein production. Crop Sci. **65**(1), e21361 (2025)
39. Jin B, Xu X. 2025 Forecasts of wholesale food price indices through Gaussian process regressions. Int J Math Ind
40. B. Jin, X. Xu, Forecasts of wholesale soybean oil price indices via gaussian process regressions. International Journal of Big Data Mining for Global Warming (2025). https://doi.org/10.1142/S2630534825500019